

Article

An Unsupervised Burned Area Mapping Approach Using Sentinel-2 Images

Michail Sismanis, Rizos-Theodoros Chadoulis , Ioannis Manakos *  and Anastasios Drosou

Centre for Research and Technology Hellas, 6th km Charilaou-Thermi Rd., 57001 Thessaloniki, Greece

* Correspondence: imanakos@iti.gr

Abstract: The frequency and severity of large, destructive fires have increased in the recent past, with extended impacts on the landscape, the human population, and ecosystems. Earth observations provide a means for the frequent, wide coverage and accurate monitoring of fire impacts. This study describes an unsupervised approach for the mapping of burned areas from Sentinel-2 satellite imagery, which is based on multispectral thresholding, and introduces an adaptive thresholding method. It takes into account the localized variability of the spectral responses in a two-phase approach. The first phase detects areas that are burned with a high probability, while the second phase adaptively adjusts this preliminary mapping by expanding and refining its boundaries. The resulting classification contains two main classes of interest: burned and unburned. The latter is further classified into four (4) fire impact severity classes, according to the Copernicus Emergency Management Service (CEMS) and the NASA United States Geological Survey (USGS)'s widely acknowledged nomenclature examples. Three distinct wildfire events are assessed, which occurred during the summers of 2020 and 2021 in Greece and Portugal. The classification accuracy is calculated by juxtaposing the classification outputs to burned area validation maps created through the photointerpretation of very high-resolution (VHR) satellite imagery. The corresponding CEMS On-Demand Mapping products are also juxtaposed against the validation maps for comparison purposes. The accuracy assessment showcases that the unsupervised approach closely follows the capacity provided by the CEMS maps (e.g., the kappa coefficient— k —of the proposed unsupervised approach is 0.91, 0.83 and 0.83 for the events processed, while the CEMS products achieve a k of 0.94, 0.93 and 0.8, respectively). The proposed approach considers the variability of the affected areas' spectral response; thus, it generalizes well to different areas, e.g., areas characterized by different land cover types. It seems to offer an effective means of mapping the wildfire-induced changes, which can be further incorporated and used by forest fire management services and further decision support systems complementary to the CEMS maps.

Keywords: burned area mapping; Sentinel-2; unsupervised thresholding; adaptive thresholding; Normalized Burn Ratio; CEMS



Citation: Sismanis, M.; Chadoulis, R.-T.; Manakos, I.; Drosou, A. An Unsupervised Burned Area Mapping Approach Using Sentinel-2 Images. *Land* **2023**, *12*, 379. <https://doi.org/10.3390/land12020379>

Academic Editor: Karel Charvat

Received: 31 December 2022

Revised: 26 January 2023

Accepted: 29 January 2023

Published: 31 January 2023



Copyright: © 2023 by the authors. Licensee MDPI, Basel, Switzerland. This article is an open access article distributed under the terms and conditions of the Creative Commons Attribution (CC BY) license (<https://creativecommons.org/licenses/by/4.0/>).

1. Introduction

Large, destructive wildfires are on the rise, ravaging communities and ecosystems in their path [1]. According to a recent analysis of data from the University of Maryland (UMD) Global Land Analysis and Discovery (GLAD) laboratory, forest fires burn almost twice as much tree cover today as they did twenty years ago [2]. Among the various driving factors responsible for this trend, anthropogenic climate change is identified as one of the most important [3]. Forest fires also have detrimental effects, causing landscape degradation [4] and soil erosion [5], increasing air pollution [6], disturbing carbon reserves [7] and affecting human populations' health [8,9].

Supporting emergency response actions in the immediate aftermath of a wildfire and developing accurate fire management strategies usually requires maps of the fire's extent and severity [10]. The potential contribution of satellite imagery was recognized early on [11,12]. Spaceborne remote sensing data can be invaluable for fire danger estimation and

prediction, fire behavior calculation, damage estimation and the monitoring of post-fire landscape recovery.

Burned area mapping at a global scale mainly relies on sensors that have a high temporal frequency (daily) but a coarse spatial resolution (such as the Moderate-Resolution Imaging Spectroradiometer—MODIS) [13–16]). A detailed review of the advantages and disadvantages of global products was performed by Chuvieco et al. [17]. Many recent studies developed burned area products utilizing high- to medium-resolution sensors, such as Sentinel-2 [18], and Landsat [19], creating products that capture details at national to regional levels [20].

A wide range of burned area mapping algorithms rely on the physics of light interaction with different materials and the identification of distinct spectral signatures. They utilize algebraic band combinations (spectral indices), such as the Normalized Burn Ratio (NBR) [21], the difference Normalized Burn Ratio (dNBR) [22,23], the Normalized Difference Vegetation Index (NDVI) [24] and the Burned Area Index for Sentinel-2 (BAIS2) [25]. Other approaches for burned area mapping rely on time series change detection [26–28] or object-based analysis [29,30]. Automatic machine learning approaches have also been used in this context: random forests [13,31,32], neural networks [33], support vector machines (SVMs) [30,34,35] and deep learning [32,36].

A two-phase approach is frequently employed for burned area detection. In the first phase, the main bulk of the burned area is detected. In the second phase, various analysis techniques are employed to improve the burned areas' estimations and delineation. Examples of methods include region growing [26,37], locally adapted multitemporal analysis [20], logistic regression [38,39] and edge detection [39]. Loboda et al. [23] proposed a three-phase approach using the dNBR for burned area mapping using MODIS data. In a similar fashion, this study describes a localized adaptive thresholding approach for burned area mapping using Sentinel-2 data to measure fire impacts on land and examine its usefulness as a complementary option to the Copernicus Emergency Management Service (CEMS) products. CEMS contains operational service chains aiming to deliver very high-accuracy products concerning disaster events in brief time windows from the service request time. CEMS disaster mapping products have been used as validation data in various approaches regarding wildfires [40–43]. Concerning catastrophic fire events, CEMS provides a set of georeferenced delineation products that contain information both for the extent of the damaged area and the area's classification into distinct classes, based on the damage severity. All products are created in a timely manner, utilizing the best resources available for the specific event. CEMS products do not rely exclusively on medium-resolution Sentinel-2 data but can leverage other very high-resolution (VHR) data, e.g., SPOT 6, based on satellite data availability. Thus, the resulting maps have a spatial resolution that is case-specific but typically is 10 m × 10 m or finer. The following damage severity classes are provided: (1) possibly damaged, (2) damaged and (3) destroyed. For the task of delineating burned areas, all three damage classes are considered burned, as per the guidelines established in [44].

This study is a follow-up of the international discussion and developments surrounding burned area mapping. Automatic mapping capacity approaches have formally been applied to image products of coarser spatial and lesser radiometric resolutions, and this study adjusts and verifies them using the latest, freely available spaceborne products of finer spatial and better radiometric resolutions. It introduces a two-phase unsupervised local thresholding approach for generating burned area maps utilizing Sentinel-2 images with acquisition dates in close temporal proximity to the fire event. The aim was to provide a surrogate automatic burned area assessment tool that complements CEMS burned area mapping products, enabling the wider coverage of events. Stakeholders and citizens, regardless of the level or the field of their expertise, would be able to benefit from it and have additional support in the decision-making processes. To evaluate its credibility, the accuracy is evaluated in comparison with state-of-the-art maps, made publicly available

by CEMS, and reference validation maps derived from the manual photointerpretation of VHR ($3\text{ m} \times 3\text{ m}$) images.

2. Materials and Methods

2.1. Earth Observation Products

Sentinel-2 Level-2A radiometrically and atmospherically corrected products provided Bottom of Atmosphere (BOA) surface reflectance input for the analysis. For each fire event assessed, a pair of images was acquired; the first image of the pair precedes the fire event, while the other follows it. Time intervals for the acceptable data acquisition window are defined in such a way as to retrieve a Sentinel-2 acquisition that is as close as possible to the date of the event. The approach also aimed to minimize variations in the physicochemical and structural conditions of dynamically changing elements of the landscape (e.g., inundation, plant communities' phenology, sun-to-object-to-sensor illumination geometry) that may influence spectral responses (histogram composition). Trial and error iterations by experimenting in the study areas led the authors to suggest and optimize time intervals for up to two Sentinel-2 overpasses before the date of the event and up to four Sentinel-2 overpasses after the date of the event, as a burn scar generally remains less changed and well detected for a longer period.

2.2. Events and Study Areas

Three distinct wildfire events were investigated. All events took place in Mediterranean regions (as shown in Figure 1), during the summer periods of 2020 and 2021. These fires were of high severity and activated the Copernicus Emergency Management Service (EMS) on-demand rapid mapping [45]. The first event took place in Barao de Sao Joao and Bordeira in Algarve, Portugal, and affected 2295 ha of land. Mainly forested areas covered with pine and eucalyptus were damaged.

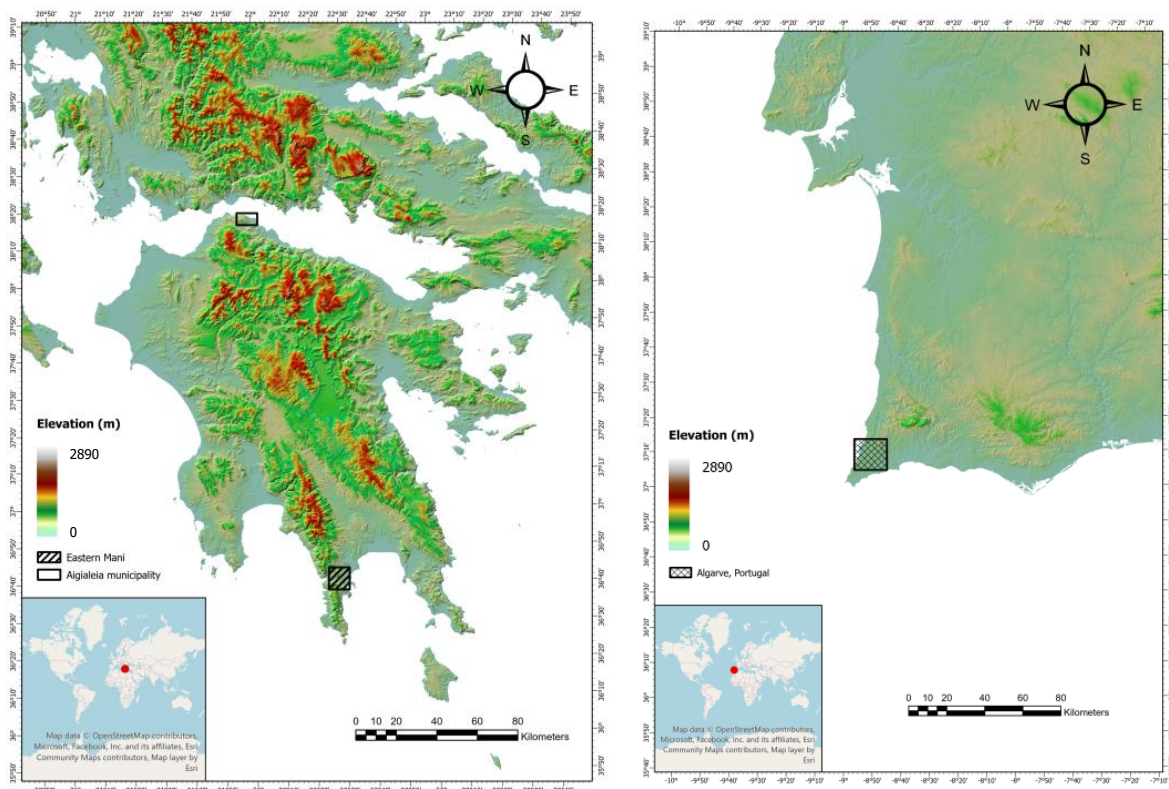


Figure 1. Maps of the three study areas: Aigialeia Municipality and Eastern Mani in Greece (**left**) and Algarve in Portugal (**right**) (on top of the Hillshaded Relief Map, which was produced from EU-DEM v1.1 [46]).

The second event took place in a forest area in Eastern Mani, Greece, where the evacuation of nearby communities was ordered by the respective authorities. The fire was considered large, damaging a total area of 1882 ha. The last event took place in Aigialeia Municipality in Greece. Forested areas were affected, along with rural and urban areas. Four (4) villages were evacuated as a precaution, and the total area affected by the fire was 395 ha.

In order to effectively minimize the noise induced by using images from different acquisition dates to produce the maps, the dates used by CEMS for creating the burned area maps were chosen as reference dates. All data used for the proposed burned area detection approach and the PlanetScope data acquisition dates used for creating the validation maps were selected based on their temporal proximity to these reference dates. If there were no Sentinel-2 images coinciding with the dates of satellite data used by CEMS, then the next closest dates were chosen, provided that the images were not hindered by cloud coverage or smoke, and there were no active fires. A detailed listing of all events and the satellite resources processed can be found in Table 1.

Table 1. List of events examined (“1” represents the event in Algarve, Portugal; “2” represents the event in Eastern Mani, Greece; “3” represents the event in Aigialeia Municipality, Greece).

Event	Approach	Event Date	Previous Image	Following Image	Satellite
1	Proposed	19/06/2020	18/06/2020	23/06/2020	Sentinel-2
1	CEMS	19/06/2020	18/06/2020	24/06/2020	SPOT6/7
1	Supervised	19/06/2020	19/06/2020	21/07/2020	Planetscope
2	Proposed	22/08/2020	16/08/2020	28/08/2020	Sentinel-2
2	CEMS	22/08/2020	16/08/2020	25/08/2020	SPOT6/7
2	Supervised	22/08/2020	17/08/2020	24/08/2020	Planetscope
3	Proposed	31/07/2021	27/07/2021	01/08/2021	Sentinel-2
3	CEMS	31/07/2021	27/07/2021	02/08/2021	SPOT6/7
3	Supervised	31/07/2021	28/07/2021	02/08/2021	Planetscope

2.3. Unsupervised Approach

The proposed approach aims at delineating burned areas by employing an unsupervised local thresholding approach that discriminates the pixels in the study area into burned and unburned classes. The flowchart of the proposed approach can be found in Figure 2. By making use of the dNBR index, the methodology proposed also offers the capacity to differentiate between different levels of damage severity based on the index values of each pixel. The damaged regions can be further divided into low severity (or possibly damaged) and moderate severity (or damaged), with these further divided into moderate–high and moderate–low severity in this study, and high severity (or destroyed), as per the established dNBR damage severity scales (as described and widely used in [10,44]).

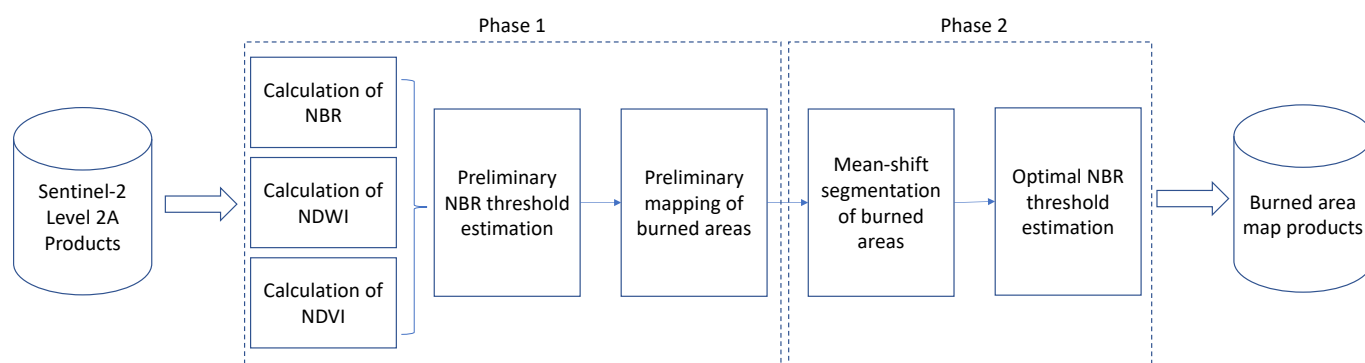


Figure 2. Flowchart diagram of the proposed approach for automatic burned area mapping.

The first phase of the unsupervised approach is to perform multispectral thresholding to detect core burned areas. Core burned areas are regions with a spectral signature indicating a high probability of fire damage. These core burned areas are then expanded to incorporate more pixels that have not been significantly damaged by the fire. This expansion is performed adaptively, considering each event's localized variability, reflectance distribution and approximate distance from the core burned area.

Preliminary tests indicated that results could be heavily influenced by noise, i.e., areas falsely detected as burned during the first detection of core burned areas. Consequently, the need arose for the establishment of noise filtering methods that can detect and exclude from the calculations all noise-afflicted areas. A noise reduction step is thus introduced to omit any potential reflectance patterns that can be regarded as burn scars, significantly impacting the subsequent steps, e.g., open surface water areas, non-vegetated areas, clouds, shadows and smoke. Open surface water areas are masked out in the post-event image using the Normalized Difference Water Index (NDWI) spectral index [47]. For the detection of non-vegetated areas, the NDVI is calculated for both the pre- and post-fire images. A pixel is classified as non-vegetated when the NDVI index value for both images is low (e.g., lower than 0.17 for the specific study areas) and its change is less than 0.04 in absolute value. This technique has been used successfully in another burned area mapping approach [48]. Clouds, shadows and smoke, which share a similar spectral signature, are masked out via the Scene Classification Layer (SCL), provided in Level 2A atmospherically corrected Sentinel-2 images by Copernicus.

Sequentially, core burned areas are detected by performing a spectral analysis on the NBR [21] index for the post-fire image. The NBR is calculated from Equation (1) using the near-infrared band (NIR) and the short-wave infrared band (SWIR), Band 08 and Band 12 of Sentinel-2, respectively. The NBR index has been selected as it is a widely used informative index for pre- and post-fire assessments on forested sites and performs well in the majority of cases [49].

$$NBR = \frac{NIR - SWIR}{NIR + SWIR} \quad (1)$$

The histogram of the NBR index after the fire (NBR_{after}) is calculated and is used to estimate an initial threshold T_{init} , which is defined as the first deep valley of the NBR_{after} histogram. T_{init} is used to perform a rough separation of the scene into core burned (low NBR) and mildly burned or unburned areas (high NBR). If a pixel p has $NBR_{after}(p) < T_{init}$, then it is classified as burned; otherwise, it is classified as unburned. As a result, an initial burned area map can be generated, containing pixels with a high probability of being burned, using the threshold T_{init} (Figure 3).

The second phase of the unsupervised approach is the segmentation of the Sentinel-2 satellite image into non-overlapping segments using the mean-shift segmentation algorithm [50]. The algorithm is given as input an image that is composed of three spectral bands: (i) Blue (Band 2), (ii) Green (Band 3) and (iii) Red (Band 4). These bands were selected on the basis of their 10 m spatial resolution, which offers a greater discrimination ability regarding the segments of the image.

The reflectances of each band are normalized to the range [0, 255]. As the minimum and maximum values of the normalized range, the 1st and the 99th percentile points of the reflectance distribution were chosen. In the case in which a reflectance intensity value is less or greater than the minimum or maximum values, then it is normalized to 0 or 255, respectively. There are two parameters of interest that affect the mean-shift segmentation algorithm, namely the spatial radius h_s and the segmentation feature space radius h_r . It has been proven in [51] that small changes in the values do not significantly affect the results. Both h_s and h_r have been empirically set equal to 3. The result of this segmentation process is a segmentation map with segments being composed of pixels that have similar spectral behavior (Figure 4). This can be also verified in [52].

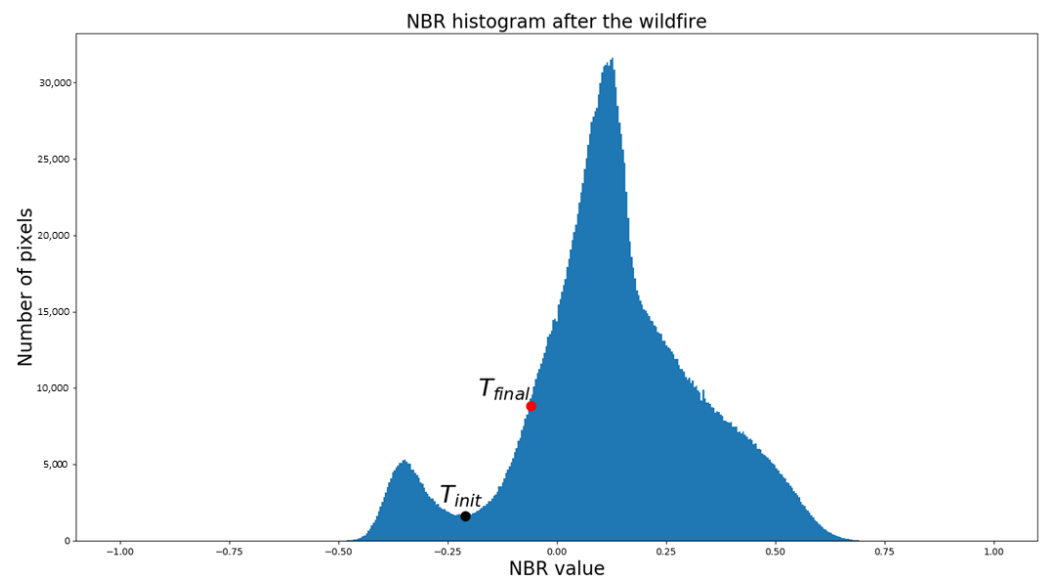


Figure 3. Histogram of the NBR index for the time instance after the fire. T_{init} is the NBR index value that corresponds to the first valley of the histogram (dot in black color). T_{final} is the threshold that is calculated after the adaptive segmentation method and will be used for the final separation of the pixels into burned and unburned classes (dot in red color).

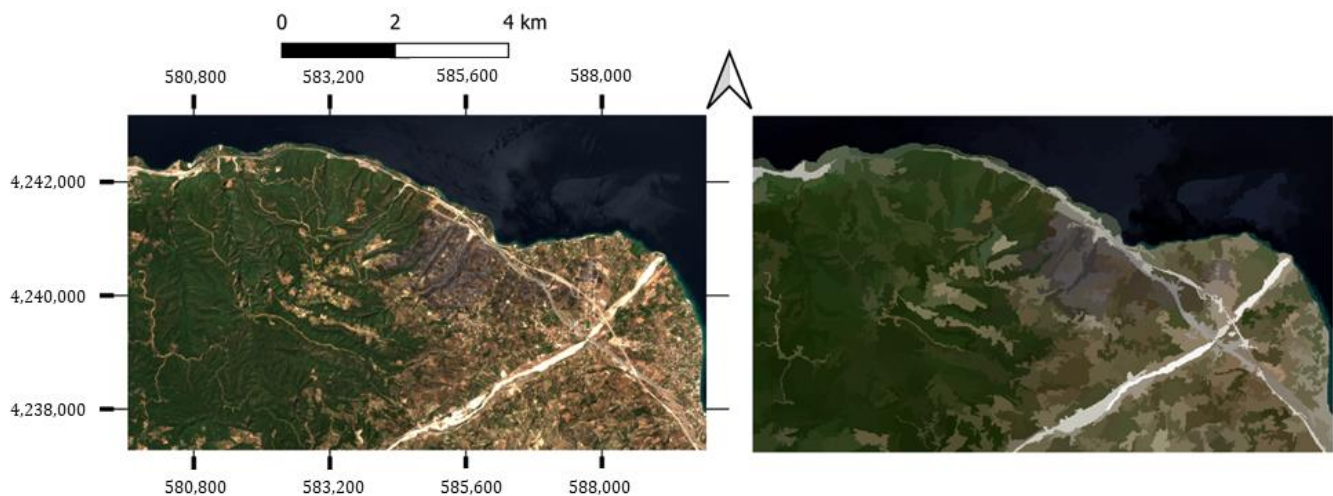


Figure 4. The post-fire RGB image of the study area in Aigialeia Municipality (left) and the segmentation map created after the application of the mean-shift algorithm (right).

The segmentation map is then subsequently utilized for detecting and selecting segments with a high percentage of burned pixels, as detected during Phase 1 by the core burned pixel classification described previously. Segments characterized by a large percentage of burned pixels ($>70\%$) are selected, and their centroids C_m are estimated. Square patches p_m^k of expanding size are centered around each C_m . The size of the square patch in pixels is calculated as $(20 \cdots k) \cdots (20 \cdots k)$, $k = 1, 2, \cdots, 20$. Using Minimum Cross-Entropy Thresholding [53], the threshold for the binary classification (i.e., burned and unburned) f_{opt}^k is estimated for a given size k . For each segment C_m , the median of all the expanding windows is considered the optimal threshold for separating burned and unburned areas. The optimal splitting threshold for the scene T_{final} is estimated as the median of all the segments' optimal thresholds (Figure 3). The final threshold T_{final} is used for a more refined classification of the area. Pixels p with $NBR_{after}(p) < T_{final}$ are considered burned. All other pixels are considered unburned. As a result, the final burned area map is

generated, containing pixels that, based on the localized approach, are considered to have a high probability of being labeled as burned.

2.4. Reference Validation Data

Reference validation data were obtained using the photointerpretation of VHR Planet multispectral imagery. A first preliminary step was implemented to assist in the process of creating the validation maps. The PlanetScope constellation of satellites provides a swarm of EO imagery with a spatial resolution of $3\text{ m} \times 3\text{ m}$. Images used in the creation of the validation dataset were acquired specifically with the PS2.SD and PSB.SD sensors operating at the Blue, Green, Red and NIR spectral bands. Using the unsupervised K-means clustering approach, a binary clustering of the areas of interest was performed into burned and unburned classes. K-means clustering aims at partitioning n observations into k sets $S = \{S_1, S_2, \dots, S_k\}$, so as to minimize the within-cluster sum of squares (WCSS). Blue, Green, Red and NIR band reflectance and NDVI values (both for the pre- and post-fire instances), along with their linear combinations, are considered as the feature data that are used for the binary clustering of the image. By clustering spectral data in a bimodal fashion, utilizing the data before and after a fire event, the detected classes for the scene depicted the two different states of the landscape: (i) pixels affected by the fire, and (ii) pixels not affected by the fire. This preliminary burned area map is used in a supportive manner, as a first rough delineation of the areas of interest that are potentially impacted by the fire. Following this, the multispectral bands and NDVI index images (pre- and post-fire) were photointerpreted by the authors on-screen and the first rough delineation map was manually refined to create the final burned area validation map.

3. Results

The maps produced from the proposed approach and the maps provided by CEMS were compared to the burned area reference maps derived from VHR data. All maps were resampled at a $3\text{ m} \times 3\text{ m}$ spatial grid resolution, matching the resolution provided by PlanetScope, minimizing cross-scale comparison errors. Two sets of comparisons were performed to assess the proposed approach's effectiveness. The first took into account results produced from the proposed approach and assessed them against the validation maps. The second set of comparisons took into account the maps provided by CEMS and assessed them against the validation maps. Comparisons were performed map-wise, with all pixels being considered and compared with their counterparts.

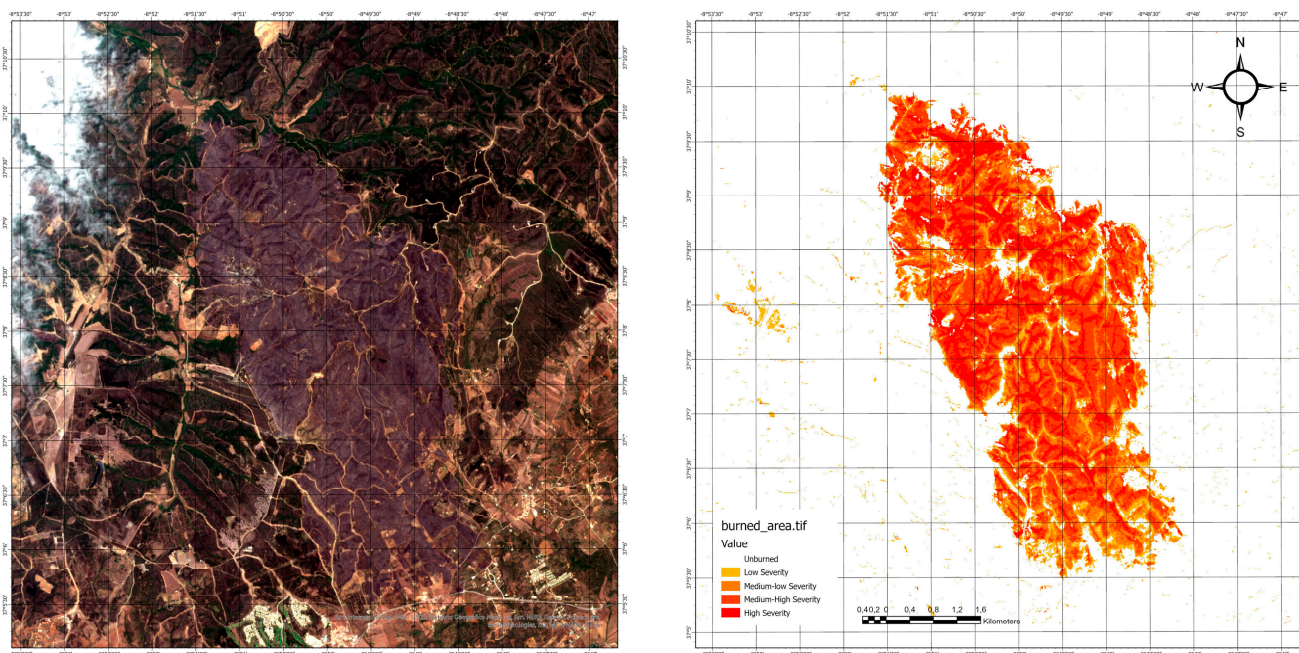
3.1. Accuracy Assessment Analysis

The accuracy estimation metrics include the estimation of the producer's accuracy (PA), user's accuracy (UA), overall accuracy (OA) and the kappa coefficient (k). UA (also known as type 1 error) is a metric providing the map user with the probability that a pixel of a class on the map represents, at that location, the same class in reality, or is the result of errors of commission, where pixels are falsely assigned to a wrong class. PA (also known as type 2 error) is a metric providing the map creator with the probability that a real location of a class appears as the same pixel class in the classification map, or is the result of errors of omission, where pixels of the target class are incorrectly classified. OA is a metric showing the probability of a classification being true. Finally, the kappa coefficient (k) is another accuracy metric that is frequently used in remote sensing applications [54], designed to include the chance agreement of the validation. Detailed accuracy assessment results can be found in Table 2.

Table 2. Accuracy metrics for all study areas per approach.

	Burned Class		Unburned Class		OA	<i>k</i>
	PA	UA	PA	UA		
Algarve—Proposed approach	92.50	90.14	99.20	99.41	98.71	0.91
Algarve—CEMS approach	90.44	98.39	99.87	99.18	99.12	0.94
Eastern Mani—Proposed approach	75.71	96.57	99.53	95.88	95.96	0.83
Eastern Mani—CEMS approach	99.58	89.14	97.81	99.92	98.08	0.93
Aigialeia—Proposed approach	80.60	87.42	99.36	98.93	98.38	0.83
Aigialeia—CEMS approach	91.85	72.87	98.11	99.54	97.78	0.80

Rows 1 and 2 present the accuracy metrics for the event in Algarve, Portugal, on 19 June 2020 (Figure 5). More specifically, the proposed approach has a PA of 92.5% and a UA of 90.14% concerning the burned class. The CEMS mapping products have a UA of 98.39% and a PA of 90.44%. Both maps' OA and *k* values are very high, with 98.71% and 0.91 for the proposed approach and 99.12% and 0.94 for CEMS, respectively. Overall, both maps display very high levels of accuracy, and the proposed approach is on par with the state-of-the-art mapping services' products.

**Figure 5.** RGB true color representation (using Sentinel-2 bands) of the wider area of Algarve, Portugal (**left**), and the burned area classified into 4 severity classes (**right**).

Rows 3 and 4 present the accuracy metrics for the fire event in Eastern Mani, Greece, on 22 August 2020. This time, the discrepancy between the proposed approach and Copernicus EMS is larger, as the proposed approach underestimates the burned area and scores 75.71% in PA and 96.57% in UA, with still a high value of 95.96% in OA (close to the 98.08% of CEMS), and a comparably lower value than the CEMS *k* at 0.83. In this event, it is evident that the PA of the proposed approach is significantly lower than that of the CEMS maps. This can be attributed to the second phase of the proposed approach, i.e., the adaptive thresholding part, which was influenced by noise present in the image, i.e., the lower left part of Figure 6. As a result, the optimal threshold was estimated in a way that prohibited the detection of certain burned areas—hence, leading to the decrease in PA.

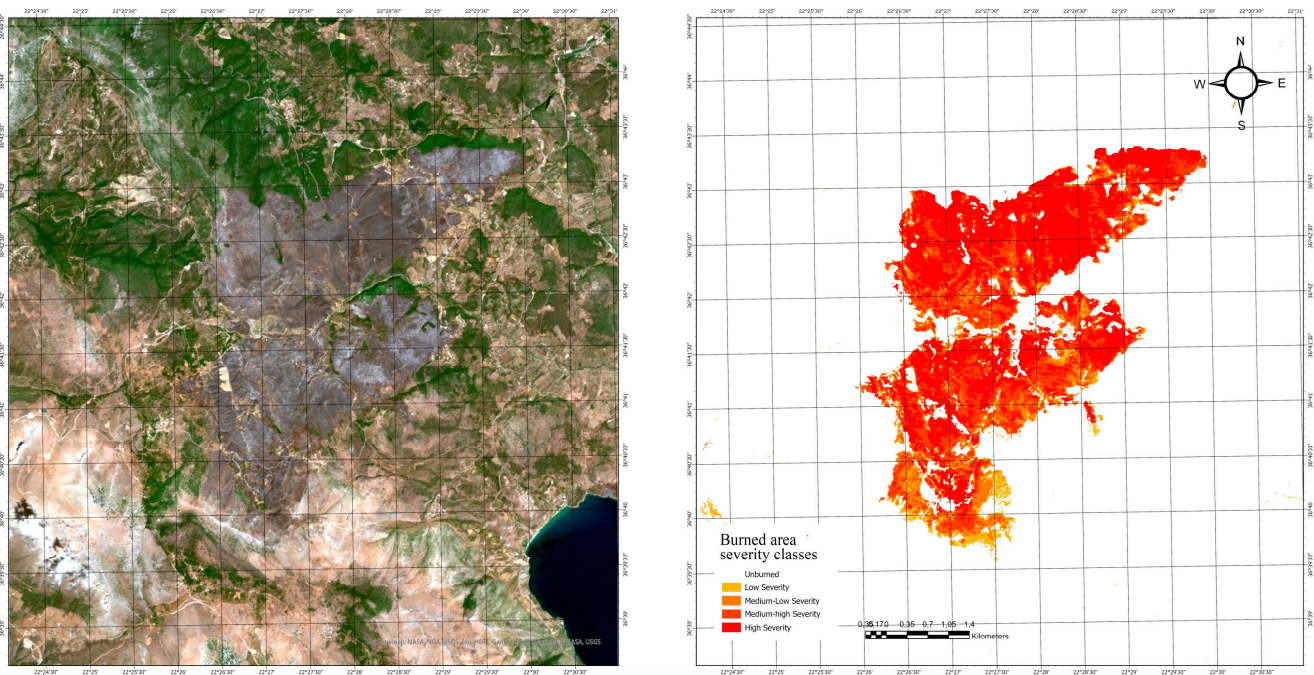


Figure 6. RGB true color representation (using Sentinel-2 bands) of the wider area of Eastern Mani, Greece (left), and the burned area classified into 4 severity classes (right).

Regarding the last event in Aigialeia Municipality in Greece (rows 5 and 6) (Figure 7), the proposed approach reaches 80.06% PA, 87.92% UA, 98.38% OA and k equal to 0.83. On the other hand, the CEMS maps achieve 91.85% PA, 72.87% UA, 97.78% OA and 0.8 k . This time, the proposed approach has underestimated, by a small margin, the burned area, while, on the other hand, the CEMS approach has overestimated the total burned area. The event in Aigialeia Municipality can be considered small in terms of the overall area affected (395 ha), with many areas ambiguous in terms of fire damage severity, which may have influenced the mapping results.



Figure 7. RGB true color representation (using Sentinel-2 bands) of the wider area of Aigialeia, Greece (left), and the burned area classified into 4 severity classes (right).

3.2. Burn Damage Severity Assessment

In this study, our focus was on the ability of the proposed approach to discriminate between burned and unburned areas. However, in view of a comparison against the benchmark results of CEMS, thresholds, suggested by USGS for dNBR interpretation [10] and adjusted by CEMS in fewer classes [44], are applied and finer fire impact severity classes could be mapped (see Figures 5–7). Classes of interest concern destroyed, damaged and possibly damaged areas. This is a more simplified scheme followed by Copernicus,

where pixels of the moderate–low- and moderate–high-severity subclasses are grouped into one class, i.e., the damaged (moderate) class [44]. In this study, both subclasses (moderate–low and moderate–high) are presented, since the suggested thresholds for both are applied and the need for a fire to be described in more detail is considered.

An assessment is then carried out to register how well the various CEMS subclasses may be re-estimated by the proposed approach (on top of the comparison presented in Section 3.1). Figure 8 shows the correlation between the impact severity classes identified by the unsupervised approach in comparison with the damage classes proposed by CEMS for each event. The following conclusions may be inferred:

- It is evident that the identified area, which is classified as showcasing a high-severity impact by the fire, is mostly evident (at approximately and more than 90%), where the CEMS destroyed class is registered. However, it can be noticed that, systematically, around 25% is misplaced to the CEMS damaged class.
- In relation to the CEMS damaged class, this is mostly identified as exhibiting moderately high (around 45–50%) or low (25–30%) impacts by the fire event. It appears that there is a match at approximately 70% between the moderate-severity subclasses (high and low) and the CEMS-nominated damaged class.
- The results become, on one hand, more distinct for the possibly damaged class, as, herein, mostly the low-severity class (at approximately 55–65%) and the moderately low-severity subclass are to be assigned (around 25–35%). The moderate–high-severity class presents a few percentage misclassifications here.
- Confusion is observed, where ambiguity becomes higher, i.e., between the low-severity class and the unburned area designation by the CEMS. Misinterpretation reaches 80–90%. Cases of moderate–low-severity (up to 12%) and moderate–high-severity (at around 1–5%) are also registered in the unburned area class.

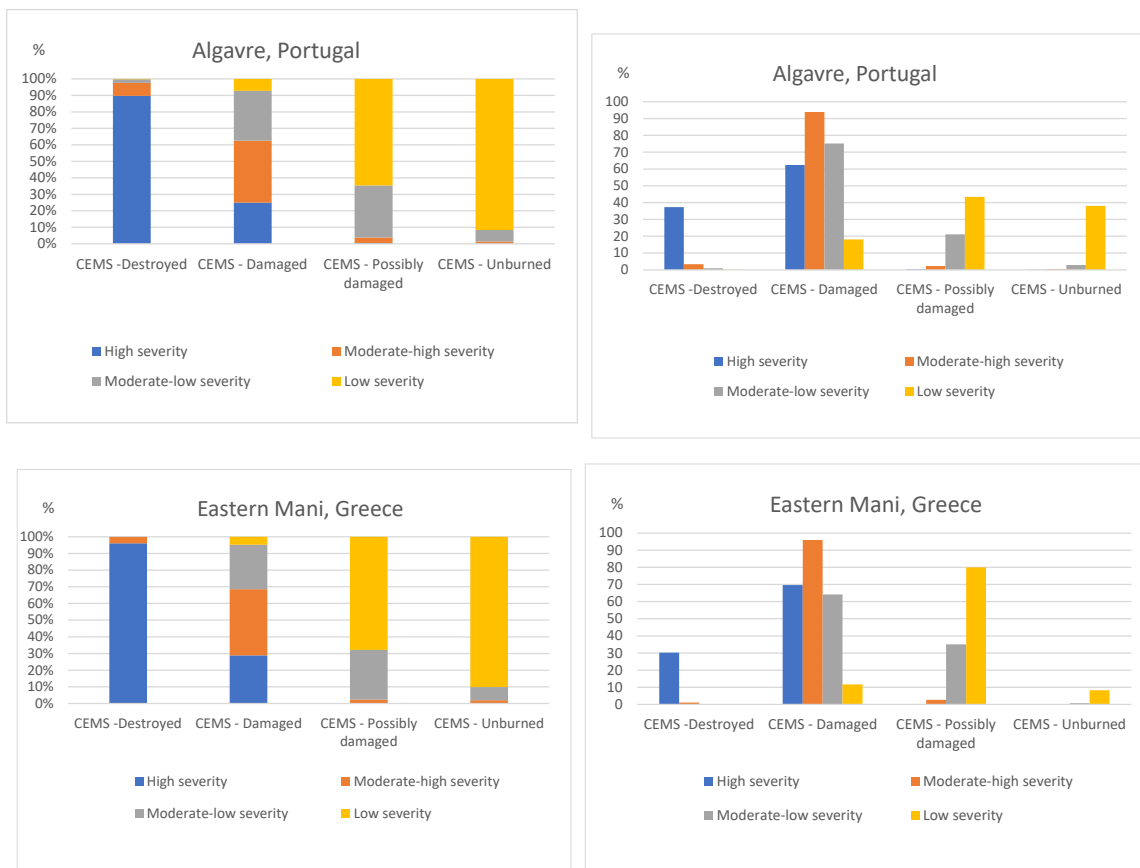


Figure 8. Cont.

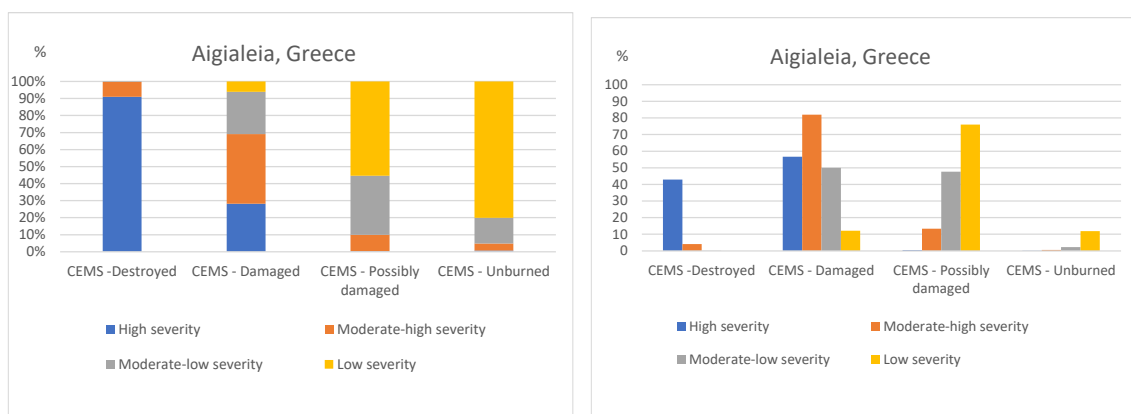


Figure 8. Contribution of the fire impact severity class as identified by the proposed approach for the identification of the relevant CEMS class (**left**), and relevance of the categorization of the proposed approach in relation to the definition merging by CEMS (**right**).

It is obvious that boundary conditions cannot be strictly defined for natural processes and an expected degree of ambiguity is present, especially across neighboring classes subdivided by strict thresholding. The aforementioned mismatches provide a detailed analysis of the local fitting between the definitions provided by CEMS, which are to be applied globally, and the outcome of the proposed approach, where the specificities of the local landscape synthesis are taken into account.

4. Discussion

Many of the proposed methods of the past years rely on multispectral data of varying spatial resolutions, i.e., MODIS, Landsat, Sentinel [13,38,43,55–57]. This work intended to leverage medium/high-resolution Sentinel-2 data and specifically address the timeliness factor of the burned area mapping processes, i.e., to deliver accurate results in a fast and efficient way, using as little data as possible, without any prior calibration [38]. This will significantly aid emergency mapping procedures, where timely reaction is of the essence and where approaches using vast time series of data would be less efficient [58].

The proposed approach has been applied to three major forest wildfire events. The overall classification accuracy of all three applications was over 90% (reaching up to 98.71%), and k was over 0.8 (reaching up to 0.91). These positive results display the potential of the proposed approach in terms of burned area mapping, as, in most cases, OA and k values approximate the validity of the results provided by CEMS, which are considered the official benchmark in the Earth observation (EO) application domain.

The first phase of the proposed approach detects core burned areas, i.e., pixels that have a spectral signature, which correlates to higher-severity changes with a very high probability. The second phase adaptively adjusts this core area by effectively expanding its boundaries, enclosing pixels of lesser severity that, based on event-specific thresholds, can be considered burned. Overall, the proposed two-phase approach has been designed with effort to minimize both errors of commission and errors of omission. While the first phase has very high detection accuracy for core burned areas (due to their distinct spectral signature), the effectiveness of the adaptive second phase is what defines, in the end, the overall accuracy of the approach. As the methodology aims to be completely automatic, errors can be possibly introduced in certain events (as is evident from some low-severity burned areas far from the main body in Figures 5 and 6). For example, dense vegetation with a high difference in moisture content between images, or artifact shadows, may produce NBR values that could potentially affect the adaptive thresholding procedure and be regarded as falsely impacted by the fire.

Previous relevant studies have also employed strict or adaptive thresholding with a multiphase approach. Of note is the work of Loboda et al. [23], who achieved values of k

ranging from 0.76 to 0.79, using a three-phase adaptive thresholding approach on MODIS data for areas across the globe. However, this performance is reported for large-area burn scars. This study's proposed adaptive thresholding approach verifies and improves these results for the undulated relief of the Mediterranean region on a larger scale (i.e., per Sentinel-2 pixel), suggesting a two-phase approach. Moreover, the self-adjusting thresholding applied by [48] seems a partially comparable approach with very good results. However, the applied Minimum Mapping Unit post-processing tends to filter out small objects, which are better targeted with this study's approach. Furthermore, this study's results indicate their comparability with alternative approaches, such as the change-point analysis-based thresholding [59], which reports a k of 0.76 utilizing Landsat-8 in Alaska, and the empirical thresholding of separability across spectral indices using spectral sensitivity analysis, achieving overall accuracies at a range of 50.1% to 96.3% for NBR across study areas in the Mediterranean [60].

The methodology presented within the scope of this work relies on an index for mapping burned areas, namely the NBR index. Other related works have used different indices in burned area mapping applications. For example, Liu et al. [28] tested several different indices in Southern Burkina Faso and observed that the Burned Area Index (BAI) performed best. The same has been deduced from the work in [38]. In [27], the authors observed that the Sentinel-2 Burned Area Index (BAI2) provided the best results when compared with other indices used in burned area mapping in a case study in Iran. The Mid-Infrared Bi-Spectral Index (MIRBI) is another index that was designed to have high sensitivity to spectral changes induced by burning and has been used in Landsat applications [61,62]. While there are indices that may display better results, either in burn scar delineation or burn damage severity assessment, the NBR (or dNBR) has always been a point of reference for burned area mapping approaches. Cocke et al. observed that the dNBR method was reliable for mapping burned areas that had been severely affected [49]. In [63], a thorough analysis of nine spectral indices was conducted, with NBR being second best in most cases.

Regarding the classification of the areas into different damage severity classes, the main obstacle was that validation maps could not be accurately provided by visual interpretation, as was possible with the distinction into burned and unburned areas. As a result, the comparison that could be performed was with the CEMS classes provided. As a result, a complete accuracy estimation for the damage severity classification of the proposed approach could not be performed. However, it seems that the distribution of the percentages into the different classes between events varies only slightly, demonstrating that the results are consistent across the various events.

The proposed automatic local thresholding approach aims at creating a burned area map detecting changes induced by wildfires at a pixel level. It enables the registration of changes affecting small areas or 'ambiguous' areas, or small patches of land that might have negligible damage. This is in line with the real situation on the ground, as fire propagation throughout the area follows a non-generalizable pattern, i.e., a region may be completely destroyed by the fire, but an adjacent minor area might be completely unaffected by the fire. The proposed approach strives to efficiently capture this dynamic, while remaining fully unsupervised. In this way, it can be of assistance to certain interested parties, i.e., civil protection or planning agencies, while at the same time requiring minimum expertise.

On the other hand, a per pixel classification scheme requires noise removal and result refinement steps to reduce commission errors and maintain PA at acceptable levels. In comparison, CEMS aims at delivering the highest-quality mapping product, in a short time window. For this purpose, semi-automatic means (supervised classification) but rarely automatic means are employed for the refinement of the results [64]. In the results presented from the proposed approach, no manual refinement has been performed. As a result, deviations can be detected in terms of accuracy, similar to those reported in other works [43]. Regarding its advantages, the proposed method is trained by the data themselves, as the optimal threshold for classifying an area regarding the burned and unburned classes of

interest is calculated in an adaptive procedure, relying on the individuality of each scene and the segments created from it. This adaptability provides a robustness to the approach, theoretically allowing credible results to be produced regardless of the image and data variability.

Through trial and error, Multilevel Minimum Cross-Entropy Thresholding (MCET) was found to best fit the purpose of this study. However, there are other thresholding approaches, such as Otsu's method [65], minimum error thresholding [66] and minmax optimization thresholding [67], that one could also employ, depending on the landscape particularities of the region.

Finally, the Sentinel-2 satellite imagery acquisition dates were chosen to be as close to the CEMS map production dates as possible, allowing for a straightforward comparison of the corresponding results. In the future, an expanded approach may be considered utilizing multiple date pairs as inputs, which are acquired at a number of pre- and post-fire instances. Such an approach could produce less noisy results, which would enhance the transferability of the approach to further areas.

5. Conclusions

In this work, an unsupervised local thresholding method was proposed for the timely generation of maps depicting areas affected by wildfire events (burn scars) from Sentinel-2 images. The proposed approach follows two phases. The first phase is to roughly detect core burned areas in the images provided, while the second phase refines estimations based on an adaptive approach. Results demonstrate that the burned areas can be mapped with very good accuracy with a pair of Sentinel-2 images, close in time to the event. The comparison with state-of-the-art maps, offered publicly by Copernicus EMS, and reference validation datasets, demonstrates that the proposed approach offers the capacity to perform mapping of the affected areas with similar overall accuracy. Therefore, it is suggested that it can be used by domain-engaged private and public sector personnel as a surrogate automatic burned area assessment tool that complements CEMS burned area mapping products. Further investigation of the automatic pixel-wise approach is suggested to assess the robustness and transferability of the method to different events and/or landscapes.

Author Contributions: Conceptualization, M.S., R.-T.C. and I.M.; methodology, M.S., R.-T.C. and I.M.; software, M.S. and R.-T.C.; validation, M.S. and R.-T.C.; formal analysis, M.S., R.-T.C. and I.M.; investigation, M.S., R.-T.C. and I.M.; resources, M.S., R.-T.C., I.M. and A.D.; data curation, M.S. and R.-T.C.; writing—original draft preparation, M.S., R.-T.C. and I.M.; writing—review and editing, M.S., R.-T.C., I.M. and A.D.; visualization, M.S., R.-T.C. and I.M.; supervision, I.M.; project administration, I.M. and A.D.; funding acquisition, I.M. and A.D. All authors have read and agreed to the published version of the manuscript.

Funding: This research has received funding from the European Union's Horizon 2020 Research and Innovation Action programme under Grant Agreement 870373-SnapEarth.

Data Availability Statement: Data partially available on request due to copyright restrictions of utilized Third Party input datasets.

Acknowledgments: The authors wish to acknowledge and thank Richard Lucas, Aberystwyth University, UK, for proofreading and helping to revise the English in the manuscript.

Conflicts of Interest: The authors declare no conflict of interest.

References

1. Sullivan, A.; Baker, E.; Kurvits, T. *Spreading Like Wildfire: The Rising Threat of Extraordinary Landscape Fires*; UNEP: Nairobi, Kenya, 2022.
2. Tyukavina, A.; Potapov, P.; Hansen, M.C.; Pickens, A.H.; Stehman, S.V.; Turubanova, S.; Parker, D.; Zalles, V.; Lima, A.; Kommareddy, I.; et al. Global Trends of Forest Loss Due to Fire From 2001 to 2019. *Front. Remote Sens.* **2022**, *3*. [[CrossRef](#)]
3. Abatzoglou, J.T.; Williams, A.P. Impact of anthropogenic climate change on wildfire across western US forests. *Proc. Natl. Acad. Sci. USA* **2008**, *113*, 11770–11775. [[CrossRef](#)] [[PubMed](#)]

4. Fernández, C.; Vega, J.A.; Fonturbel, T.; Pérez-Gorostiaga, P.; Jiménez, E.; Madrigal, J. Effects of wildfire, salvage logging and slash treatments on soil degradation. *Land Degrad. Dev.* **2007**, *18*, 591–607. [[CrossRef](#)]
5. Alloza, J.A.; Baeza, M.J.; De la Riva, J.; Duguy, B.; Echeverr, M.T.; Ibarra, P.; Llovet, J.; Perez-Cabello, F.; Rovira, P.; Vallejo, V.R. A model to evaluate the ecological vulnerability to forest fires in Mediterranean ecosystems. *For. Ecol. Manag.* **2006**, *234*, S203. [[CrossRef](#)]
6. Wu, J.; Kong, S.; Wu, F.; Cheng, Y.; Zheng, S.; Yan, Q.; Zheng, H.; Yang, G.; Zheng, M.; Liu, D.; et al. Estimating the open biomass burning emissions in central and eastern China from 2003 to 2015 based on satellite observation. *Atmos. Chem. Phys.* **2006**, *18*, 11623–11646. [[CrossRef](#)]
7. Bowman, D.M.J.S.; Balch, J.K.; Artaxo, P.; Bond, W.J.; Carlson, J.M.; Cochrane, M.A.; D’Antonio, C.M.; DeFries, R.S.; Doyle, J.C.; Harrison, S.P.; et al. Fire in the Earth System. *Science (N. Y.)* **2009**, *324*, 481–484. [[CrossRef](#)]
8. Nguyen, H.D.; Azzi, M.; White, S.; Salter, D.; Trieu, T.; Morgan, G.; Rahman, M.; Watt, S.; Riley, M.; Chang, L.T.-C.; et al. The Summer 2019–2020 Wildfires in East Coast Australia and Their Impacts on Air Quality and Health in New South Wales, Australia. *Int. J. Environ. Res. Public Health* **2021**, *18*, 3538. [[CrossRef](#)]
9. Cascio, W.E. Wildland fire smoke and human health. *Sci. Total Environ.* **2018**, *624*, 586–595. [[CrossRef](#)]
10. Keeley, J.E. Fire intensity, fire severity and burn severity: A brief review and suggested usage. *Int. J. Wildland Fire* **2009**, *18*, 116–126. [[CrossRef](#)]
11. Jayaweera, K.O.L.F.; Ahlnas, K. Detection of thunderstorms from satellite imagery for forest fire control. *J. For.* **1974**, *72*, 768–770.
12. Gutman, G.; Bartalev, S.; Korovin, G. Delineation of large fire damage areas in boreal forests using NOAA AVHRR measurements. *Adv. Space Res.* **1995**, *15*, 111–113. [[CrossRef](#)]
13. Ramo, R.; Chuvieco, E. Developing a Random Forest algorithm for MODIS global burned area classification. *Remote Sens.* **2017**, *9*, 1193. [[CrossRef](#)]
14. Giglio, L.; Descloitres, J.; Justice, C.O.; Kaufman, Y.J. An Enhanced Contextual Fire Detection Algorithm for MODIS. *Remote Sens. Environ.* **2003**, *87*, 273–282. [[CrossRef](#)]
15. Roy, D.P.; Jin, Y.; Lewis, P.E.; Justice, C.O. Prototyping a global algorithm for systematic fire-affected area mapping using MODIS time series data. *Remote Sens. Environ.* **2005**, *97*, 137–162. [[CrossRef](#)]
16. Giglio, L.; Van der Werf, G.R.; Randerson, J.T.; Collatz, G.J.; Kasibhatla, P. Global estimation of burned area using MODIS active fire observations. *Atmos. Chem. Phys.* **2006**, *6*, 957–974. [[CrossRef](#)]
17. Chuvieco, E.; Mouillot, F.; van der Werf, G.R.; Miguel, J.S.; Tanase, M.; Koutsias, N.; García, M.; Yebra, M.; Padilla, M.; Gitas, I.; et al. Historical background and current developments for mapping burned area from satellite Earth observation. *Remote Sens. Environ.* **2019**, *225*, 45–64. [[CrossRef](#)]
18. Drusch, M.; Del Bello, U.; Carlier, S.; Colin, O.; Fernandez, V.; Gascon, F.; Hoersch, B.; Isola, C.; Laberinti, P.; Martimort, P.; et al. Sentinel-2: ESA’s Optical High-Resolution Mission for GMES Operational Services. *Remote Sens. Environ.* **2012**, *120*, 25–36. [[CrossRef](#)]
19. Loveland, T.R.; Dwyer, J.L. Sentinel-2: Landsat: Building a strong future. *Remote Sens. Environ.* **2012**, *122*, 22–29. [[CrossRef](#)]
20. Roteta, E.; Bastarrika, A.; Padilla, M.; Storm, T.; Chuvieco, E. Development of a Sentinel-2 burned area algorithm: Generation of a small fire database for sub-Saharan Africa. *Remote Sens. Environ.* **2019**, *222*, 1–17. [[CrossRef](#)]
21. Benson, N.; Key, C.H.; Northern, U.; Mountain, R.; Benson, N.C.; Glacier, U.; Park, N. Measuring and remote sensing of burn severity: The CBI and NBR. In Proceedings of the Joint Fire Science Conference and Workshop, Boise, ID, USA, 15–17 June 1999; pp. 15–17.
22. Miller, J.D.; Thode, A.E. Quantifying burn severity in a heterogeneous landscape with a relative version of the delta Normalized Burn Ratio (dNBR). *Remote Sens. Environ.* **2007**, *109*, 66–80. [[CrossRef](#)]
23. Loboda, T.; O’neal, K.J.; Csiszar, I. Regionally adaptable dNBR-based algorithm for burned area mapping from MODIS data. *Remote Sens. Environ.* **2007**, *109*, 429–442. [[CrossRef](#)]
24. Chuvieco, E.; Martin, M.P.; Palacios, A. Assessment of different spectral indices in the red-near-infrared spectral domain for burned land discrimination. *Int. J. Remote Sens.* **2002**, *23*, 5103–5110. [[CrossRef](#)]
25. Filipponi, F. BAIS2: Burned Area Index for Sentinel-2. *Proceedings* **2018**, *2*, 364.
26. Hardtke, L.A.; Blanco, P.D.; del Valle, H.F.; Metternicht, G.I.; Sione, W.F. Semi-automated mapping of burned areas in semi-arid ecosystems using MODIS time-series imagery. *Int. J. Appl. Earth Obs. Geoinf.* **2015**, *38*, 25–35. [[CrossRef](#)]
27. Farhadi, H.; Mokhtarzade, M.; Ebadi, H.; Asghari Beirami, B. Rapid and automatic burned area detection using sentinel-2 time-series images in google earth engine cloud platform: A case study over the Andika and Behbahan Regions, Iran. *Environ. Monit. Assess.* **2022**, *194*, 369. [[CrossRef](#)]
28. Liu, J.; Maeda, E.E.; Wang, d.; Heiskanen, J. Sensitivity of Spectral Indices on Burned Area Detection using Landsat Time Series in Savannas of Southern Burkina Faso. *Remote Sens.* **2021**, *13*, 2492. [[CrossRef](#)]
29. Katagis, T.; Gitas, I.Z.; Mitri, G.H. An object-based approach for fire history reconstruction by using three generations of landsat sensors. *Remote Sens.* **2014**, *6*, 5480–5496. [[CrossRef](#)]
30. Dragozi, E.; Gitas, I.Z.; Stavroudis, D.G.; Theocharis, J.B. Burned area mapping using support vector machines and the FuzCoC feature selection method on VHR IKONOS imagery. *Remote Sens.* **2014**, *6*, 12005–12036. [[CrossRef](#)]
31. Gibson, R.; Danaher, T.; Hehir, H.; Collins, L. A remote sensing approach to mapping fire severity in south-eastern Australia using sentinel 2 and random forest. *Remote Sens. Environ.* **2020**, *240*, 111702. [[CrossRef](#)]

32. Lee, C.; Park, S.; Kim, T.; Liu, S.; Md Reba, M.N.; Oh, J.; Han, Y. Machine Learning-Based Forest Burned Area Detection with Various Input Variables: A Case Study of South Korea. *Appl. Sci.* **2022**, *12*, 10077. [[CrossRef](#)]
33. Ba, R.; Song, W.; Li, X.; Xie, Z.; Lo, S. Integration of multiple spectral indices and a neural network for burned area mapping based on MODIS data. *Remote Sens.* **2019**, *11*, 326. [[CrossRef](#)]
34. Cao, X.; Chen, J.; Matsushita, B.; Imura, H.; Wang, L. An automatic method for burn scar mapping using support vector machines. *Int. J. Remote Sens.* **2009**, *30*, 577–594. [[CrossRef](#)]
35. Pereira, A.A.; Pereira, J.M.; Libonati, R.; Oom, D.; Setzer, A.W.; Morelli, F.; Machado-Silva, F.; De Carvalho, L.M.T. Burned area mapping in the Brazilian Savanna using a one-class support vector machine trained by active fires. *Remote Sens.* **2017**, *9*, 1161. [[CrossRef](#)]
36. Knopp, L.; Wieland, M.; Rättich, M.; Martinis, S. A deep learning approach for burned area segmentation with Sentinel-2 data. *Remote Sens.* **2020**, *12*, 2422. [[CrossRef](#)]
37. Lizundia-Loiola, J.; Otón, G.; Ramo, R.; Chuvieco, E. A spatio-temporal active-fire clustering approach for global burned area mapping at 250m from MODIS data. *Remote Sens. Environ.* **2020**, *236*, 111493. [[CrossRef](#)]
38. Bastarrika, A.; Chuvieco, E.; Martín, M.P. Mapping burned areas from landsat TM/ETM+ data with a two-phase algorithm: Balancing omission and commission errors. *Remote Sens. Environ.* **2011**, *115*, 1003–1012. [[CrossRef](#)]
39. Bastarrika, A.; Chuvieco, E.; Martín, M.P. Automatic burned land mapping from MODIS time series images: Assessment in Mediterranean ecosystems. *IEEE Trans. Geosci. Remote Sens.* **2011**, *49*, 3401–3413. [[CrossRef](#)]
40. Filipponi, F. Exploitation of sentinel-2 time series to map burned areas at the national level: A case study on the 2017 Italy wildfires. *Remote Sens.* **2019**, *11*, 622. [[CrossRef](#)]
41. Navarro, G.; Caballero, I.; Silva, G.; Parra, P.C.; Vázquez, Á.; Caldeira, R. Evaluation of forest fire on Madeira Island using Sentinel-2A MSI imagery. *Int. J. Appl. Earth Obs. Geoinf.* **2017**, *58*, 97–106. [[CrossRef](#)]
42. Fernández-Manso, A.; Fernández-Manso, O.; Quintano, C. SENTINEL-2A red-edge spectral indices suitability for discriminating burn severity. *Int. J. Appl. Earth Obs. Geoinf.* **2016**, *50*, 170–175. [[CrossRef](#)]
43. Kovács, K.D. Evaluation of burned areas with sentinel-2 using snap: The case of kineta and mati, Greece, July 2018. *Geogr. Tech.* **2019**, *14*, 20–38. [[CrossRef](#)]
44. Emergency Mapping Guidelines—Fire Mapping Chapter. Available online: https://www.un-spider.org/sites/default/files/IWG_SEM_Guidelines_Fire_chapter_SERTIT_2_0.pdf (accessed on 20 January 2023).
45. Copernicus Emergency Management Service. Available online: <https://emergency.copernicus.eu/> (accessed on 20 January 2023).
46. EU-DEM v1.1—Copernicus Land Monitoring Service. Available online: <https://land.copernicus.eu/imagery-in-situ/eu-dem/eu-dem-v1.1> (accessed on 29 December 2022).
47. McFeeters, S.K. The use of the Normalized Difference Water Index (NDWI) in the delineation of open water features. *Int. J. Remote Sens.* **1996**, *17*, 1425–1432. [[CrossRef](#)]
48. Wozniak, E.; Aleksandrowicz, S. Self-adjusting thresholding for burnt area detection based on optical images. *Remote Sens.* **2019**, *11*, 2669. [[CrossRef](#)]
49. Cocke, A.E.; Fulé, P.Z.; Crouse, J.E. Comparison of burn severity assessments using Differenced Normalized Burn Ratio and ground data. *Int. J. Wildland Fire* **2005**, *14*, 189–198. [[CrossRef](#)]
50. Comaniciu, D.; Meer, P. Mean Shift: A Robust Approach Toward Feature Space Analysis. *IEEE Trans. Pattern Anal. Mach. Intell.* **2002**, *24*, 603–619. [[CrossRef](#)]
51. Kordelas, G.A.; Manakos, I.; Aragonés, D.; Díaz-Delgado, R.; Bustamante, J. Fast and automatic data-driven thresholding for inundation mapping with Sentinel-2 data. *Remote Sens.* **2018**, *10*, 910. [[CrossRef](#)]
52. Tombari, F.; Mattoccia, S.; Di Stefano, L. Segmentation-Based Adaptive Support for Accurate Stereo Correspondence. In Proceedings of the Pacific-Rim Symposium on Image and Video Technology, Santiago, Chile, 17–19 December 2007; pp. 427–438.
53. Li, C.H.; Lee, C.K. Minimum cross entropy thresholding. *Pattern Recognit.* **1993**, *26*, 4. [[CrossRef](#)]
54. Congalton, R.G.; Oderwald, R.G.; Mead, R.A. Assessing Landsat classification accuracy using discrete multivariate analysis statistical techniques. *Photogramm. Eng. Remote Sens.* **1983**, *49*, 1671–1678.
55. Roy, D.P.; Huang, H.; Boschetti, L.; Giglio, L.; Yan, L.; Zhang, H.H.; Li, Z. Landsat-8 and Sentinel-2 burned area mapping—A combined sensor multi-temporal change detection approach. *Remote Sens. Environ.* **2019**, *231*, 111254. [[CrossRef](#)]
56. Ngadze, F.; Mpakairi, K.S.; Kavhu, B.; Ndaimani, H.; Maremba, M.S. Exploring the utility of Sentinel-2 MSI and Landsat 8 OLI in burned area mapping for a heterogenous savannah landscape. *PLoS ONE* **2020**, *15*, e0232962. [[CrossRef](#)] [[PubMed](#)]
57. Huang, H.; Roy, D.P.; Boschetti, L.; Zhang, H.K.; Yan, L.; Kumar, S.S.; Gomez-Dans, J.; Li, J. Separability analysis of Sentinel-2A Multi-Spectral Instrument (MSI) data for burned area discrimination. *Remote Sens.* **2016**, *8*, 873. [[CrossRef](#)]
58. Hawbaker, T.J.; Vanderhoof, M.K.; Beal, Y.J.; Takacs, J.D.; Schmidt, G.L.; Falgout, J.T.; Williams, B.; Fairaux, N.M.; Caldwell, M.K.; Picotte, J.J.; et al. Mapping burned areas using dense time-series of Landsat data. *Remote Sens. Environ.* **2017**, *198*, 504–522. [[CrossRef](#)]
59. Gholinejad, S.; Khesali, E. An automatic procedure for generating burn severity maps from the satellite images-derived spectral indices. *Int. J. Digit. Earth* **2021**, *14*, 1659–1673. [[CrossRef](#)]
60. Smiraglia, D.; Filipponi, F.; Mandrone, S.; Tornato, A.; Taramelli, A. Agreement Index for Burned Area Mapping: Integration of Multiple Spectral Indices Using Sentinel-2 Satellite Images. *Remote Sens.* **2020**, *12*, 1862. [[CrossRef](#)]

61. Trigg, S.; Flasse, S. An evaluation of different bi-spectral spaces for discriminating burned shrub-savannah. *Int. J. Remote Sens.* **2001**, *22*, 2641–2647. [[CrossRef](#)]
62. McCarley, T.R.; Smith, A.M.; Kolden, C.A.; Kreitler, J. Evaluating the Mid-Infrared Bi-spectral Index for improved assessment of low-severity fire effects in a conifer forest. *Int. J. Wildland Fire* **2018**, *27*, 407–412. [[CrossRef](#)]
63. Liu, S.; Zheng, Y.; Dalponte, M.; Tong, X. A novel fire index-based burned area change detection approach using Landsat-8 OLI data. *Eur. J. Remote Sens.* **2020**, *53*, 104–112. [[CrossRef](#)]
64. Joubert-Boitat, I.; Wania, A.; Dalmaso, S. *Manual for CEMS-Rapid Mapping Products, EUR 30370 EN*; Publications Office of the European Union: Luxembourg, 2020; ISBN 978-92-76-21683-4.
65. Otsu, N. A Threshold Selection Method from Gray-Level Histograms. *IEEE Trans. Syst. Man Cybern.* **1979**, *9*, 62–66. [[CrossRef](#)]
66. Kittler, J.; Illingworth, J. Minimum error thresholding. *Pattern Recognit.* **1986**, *19*, 41–47. [[CrossRef](#)]
67. Saha, B.N.; Ray, N. Image thresholding by variational minimax optimization. *Pattern Recognit.* **2009**, *42*, 843–856. [[CrossRef](#)]

Disclaimer/Publisher’s Note: The statements, opinions and data contained in all publications are solely those of the individual author(s) and contributor(s) and not of MDPI and/or the editor(s). MDPI and/or the editor(s) disclaim responsibility for any injury to people or property resulting from any ideas, methods, instructions or products referred to in the content.